Characteristics and sources of volatile organic compounds (VOCs) in Shanghai during summer: Implications of regional transport

Yuehui Liu[a,b], Hongli Wang[b,*], Shengao Jing[b], Yaqin Gao[b], Yarong Peng[a,b], Shengrong Lou[b], Tiantao Cheng[c,d,**], Shikang Tao[b], Li Li[b], Yingjie Li[b], Dandan Huang[b], Qian Wang[b], Jingyu An[b]

[a] Shanghai Key Laboratory of Atmospheric Particle Pollution and Prevention (LAP³), Department of Environmental Science and Engineering, Institute of Atmospheric Sciences, Fudan University, Shanghai, 200438, China
[b] State Environmental Protection Key Laboratory of Formation and Prevention of Urban Air Pollution Complex, Shanghai Academy of Environmental Sciences, Shanghai, 200233, China
[c] Department of Atmospheric and Oceanic Sciences, Institute of Atmospheric Sciences, Fudan University, Shanghai, 200438, China
[d] Shanghai Institute of Eco-Chongming (SIEC), Shanghai, 200062, China

GRAPHICAL ABSTRACT
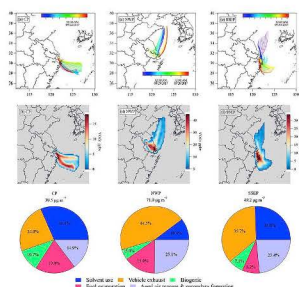
ARTICLE INFO

ABSTRACT

Intensive field measurements were carried out in urban Shanghai between 20th and 30th of May 2017, and the VOC characteristics and sources were investigated with a focus on the relative contributions of local emissions and regional transport, as well as on the potential source regions. The VOC characteristics and sources largely depended on the meteorological conditions, especially wind direction and wind speed. Generally, two kinds of episodes were associated with regional transport. In one scenario, pollutants were transported from areas upwind (north-to-northwest) of Shanghai, specifically the Suzhou-Wuxi-Changzhou and Nantong city clusters and were characterized by combustion emissions and aged air masses. In the other scenario, pollutants were transported from areas upwind (south-to-southeast) of Shanghai, specifically Ningbo-Zhoushan port, and were characterized by industrial emissions and aged air masses. Additionally, an episode associated with air masses from the clean area over the sea provided an opportunity to study the local emissions of VOCs in Shanghai. Vehicle exhaust and chemical industries, especially solvent usage, contributed a majority of the VOCs in urban Shanghai in summer, together accounting for more than 55%. The aromatic fraction of the PAMS in Shanghai was significantly higher than that in other regions in China. Regional transport and secondary formation were also important sources of VOCs, and their contribution ranged from ~15% to ~25% depending on the meteorological conditions, with an hourly maximum contribution as high as 67%. Fuel evaporation, especially

* Corresponding author.
** Corresponding author. Department of Atmospheric and Oceanic Sciences, Institute of Atmospheric Sciences, Fudan University, Shanghai 200438, China.
E-mail addresses: wanghl@saes.sh.cn (H. Wang), ttcheng@fudan.edu.cn (T. Cheng).

leakage emissions, should be addressed in Shanghai. The present study highlights the fact that joint control of VOCs in conjunction with surrounding cities is critical for Shanghai.

1. Introduction

Volatile organic compounds (VOCs) include a wide range of common atmospheric organic chemicals and can cause acute or chronic health effects. VOCs play significant roles in the formation of secondary organic aerosol (SOA) and ground-level ozone (O_3) (Atkinson, 2000; Seinfeld and Pandis, 2016). Furthermore, VOCs have numerous sources, making them ubiquitous. Many of the sources at a given location include both biogenic (Liu et al., 2018b; Wagner and Kuttler, 2014) and anthropogenic emissions, such as those from vehicles (Gentner et al., 2013), industries (Chan et al., 2006; Zheng et al., 2017a), and secondary formation due to oxidation (Spaulding et al., 2003; Yang et al., 2018). However, VOCs can also experience regional transport over distances of up to hundreds of kilometers (Lindaas et al., 2017; Zheng et al., 2017b). Therefore, the measured concentrations of VOCs are influenced by both local emissions and regional sources via transport (Geng et al., 2011; Guo et al., 2006; Liu et al., 2008b). The importance of VOCs as precursors and the ubiquity of their sources have resulted in considerable interest in the contribution of regional transport to atmospheric VOC concentrations (Guo et al., 2009; Wei et al., 2018; Zhang et al., 2008).

Shanghai is one of the megacities in Asia, with a population of over 24.1 million and more than 3.9 million motor vehicles (Shanghai Municipal Statistics Bureau, 2018). Because Shanghai is at the center of the city clusters in the Yangtze River Delta (YRD) in eastern China, the regional transport of air pollution is an important factor (Li et al., 2019b). Studies have been shown that the formation of O_3 in urban Shanghai is limited by VOCs (Geng et al., 2011; Ran et al., 2009; Tie et al., 2013; Xue et al., 2014). These previous studies have rarely focused on the spatial and temporal variations, and source characteristics of VOCs in urban Shanghai, combined with air masses transported from areas upwind of Shanghai (Chan et al., 2017). Understanding the relationship of VOCs between the upwind areas of Shanghai and the urban areas of Shanghai during O_3 pollution, is of great significance for understanding their atmospheric chemistry and mitigating these air pollutants. Therefore, it is essential to accurately illustrate how the characteristics of air masses varied with upwind areas of Shanghai, especially in terms of the contribution from regional transport to ambient VOC concentrations in urban Shanghai.

In this study, a field campaign was carried out in urban Shanghai from 20th to 30th of May 2017. A total of 108 VOC species, ozone and other trace gases and meteorological parameters were continuously observed simultaneously. Three typical kinds of episodes were identified mainly based on the meteorological conditions. The VOC characteristics and sources were investigated during the different episodes. The concentration weighted trajectory (CWT) approach was used to locate source areas potentially affecting the VOC concentrations in Shanghai.

2. Method

2.1. Sampling site

The sampling site is on the rooftop of a five-story building at the Shanghai Academy of Environmental Sciences (SAES, 31°17′ N, 121°43′ E), located in the Xuhui district near the center of Shanghai city (see Fig. S1). As shown in Fig. S1, the sampling site is in a typical residential and commercial area, with straight-line distances of 500 m east to the Humin Elevated Road and 150 m south to the Caobao Road. No apparent industrial sources present in the vicinity of the sampling site.

Therefore, the SAES site is representative of a typical urban environment in Shanghai. Detailed information on the representative of the sampling site and period are provided in Table S1 and Fig. S2 in section S1. The Shanghai Jinshan Industrial Park is approximately 50 km southwest of the SAES site (Ran et al., 2009). Almost 150 km south-southeast of the SAES site is the Ningbo-Zhoushan port, wherein petrochemical industrial parks, as well as marine mobile sources or commercial marine vessels emissions, are situated. Apart from these, in the south of Shanghai and the Ningbo city, there are large broad-leaved forests (Geng et al., 2011; Guo et al., 2013) associated with high biogenic emissions (Geng et al., 2011); marine phytoplankton distribution in eutrophic coastal and upwelling regions in the East China Sea (Li et al., 2017a), is the major contributor to marine isoprene emissions. During summertime, atmospheric pollutants are more likely to originate from local emissions and regional transport. The potential sources may affect the VOCs measured at the SAES site under certain meteorological conditions.

2.2. VOC measurements

A custom-built online gas chromatography system equipped with a mass spectrometer and a flame ionization detector (GC-MS/FID) was used for monitoring ambient alkanes, alkenes, acetylene, aromatics, halogenated hydrocarbons (XVOCs) and oxygenated VOCs (OVOCs). This system was described in Wang et al. (2014). The VOC Standards U.S. EPA PAMS mixture (provided by Spectra Gases Inc., USA) was applied in the calibration of PAMS species. Other VOC species were quantified by oxygen standard mixture gas (compendium method TO15) and then classified into OVOCs and XVOCs (EPA, 1999). Bromochloromethane, 1,4-difluorobenzene, chlorobenzene and 4-bromofluorobenzene were used as internal standards for MS calibration. Detailed information on quality assurance and quality control (QA/QC) procedures and their corresponding results are presented in section S1 and Fig. S3.

Formaldehyde was measured by a commercial Aero-Laser (AL4021) based on the Hantzsch (acetyl-acetone) reaction (Nash, 1953), which has shown high stability (Preunkert et al., 2013). The detection limit of the instrument was below 0.05 ppbv, and the temporal resolution was 1 min. The maximum range of formaldehyde was approximately 30 ppbv. Finally, all 108 VOC species were identified and quantified, as listed in Table S2.

2.3. Other measurements

Gaseous pollutants (NO–NO_2-NO_x, SO_2, CO and O_3) were measured with 1 min time resolution. Instruments (Thermo Scientific™ 42i, 43i-TLE, 48i-TLE and 49i) were manually calibrated by the zero/span checks every week. The detection limits are 0.40 ppbv, 0.50 ppbv, 0.04 ppmv and 0.50 ppbv, respectively. In addition, peroxyacetyl nitrate (PAN) was measured using an online gas chromatograph-electron capture detector (PANs-1000, Focused Photonics Inc., Hangzhou, China) with a time resolution of 5 min and a detection limit of 0.05 ppbv, which was manually calibrated by the two-point (i.e., 4.0 and 8.0 ppbv, respectively) checks every week with an analytical deviation of less than 5%. Meteorological variables, such as temperature (T), relative humidity (RH), wind speed (WS) and wind direction (WD), were synchronously acquired at a weather station about 10 km northwest of the SAES site (https://www.wunderground.com/); solar radiation (R_s) from the SAES site.

2.4. Concentration weighted trajectory (CWT)

In this study, a CWT approach was used to source areas potentially affecting the VOC concentrations in Shanghai. The CWT analysis is based on hourly VOC concentration data, and the residence time of a back trajectory arriving at Shanghai in each grid cell is determined via Equation (1):

$$CWT_{ij} = \frac{\sum_{L=1}^{M} C_L \tau_{ij-L}}{\sum_{L=1}^{M} \tau_{ij-L}} \tag{1}$$

where CWT_{ij} is the attributed VOC concentrations in the ij^{th} grid cell, L is the index of the trajectory, M is the total number of back trajectories over a time period, C_L is the 1 h VOC concentration corresponding to the arrival of back trajectory L, τ_{ij-L} is the number of trajectory segment endpoints in grid cell (i, j) for back trajectory L divided by the total number of trajectory segment endpoints for back trajectory L.

To consider air parcels with good representativeness, a weighted function has been added to the calculation to downweight cells associated with low values of n_{ij}. The method applied in ZeFir (Petit et al., 2017) was based on the trajectory density by calculating $\log(n+1)$, as described by Bressi et al. (2014) and Waked et al. (2014). The weighted function is empirically determined as follows:

$$W = \begin{cases} 1 & \text{for } \log(n+1) > 0.85_* \max_{\log(n+1)} \\ 0.725 & \text{for } 0.6_* \max_{\log(n+1)} < \log(n+1) \, 0.85_* \max_{\log(n+1)} \\ 0.475 & \text{for } 0.35_* \max_{\log(n+1)} < \log(n+1) \, 0.6_* \max_{\log(n+1)} \\ 0.175 & \text{for } \log(n+1) < 0.35_* \max_{\log(n+1)} \end{cases} \tag{2}$$

Finally, the spatial coverage of the grid cells was set from 25 to 40°N

and from 112 to 130°E, with a grid resolution of 0.2° × 0.2°. In addition, a smoothing factor (i.e., the strength of the Gaussian filter for the attributed contributions) of 2 was applied in the present study.

2.5. Positive matrix factorization model

Positive matrix factorization (PMF) has been widely used to determine and quantify the contribution of sources to samples based on the chemical composition or the fingerprint of targeted sources (Paatero, 1999; Paatero and Tapper, 1994). A total of 30 VOC species were selected for the PMF application, and a detailed description can be found in section S2. Factor contributions and profiles are derived by the PMF model. In accordance with the method recommended by the U.S. EPA PMF 5.0 (Norris et al., 2014), the uncertainty (Unc) file is calculated based on a user provided fraction of the concentration and method detection limit (MDL) (Polissar et al., 1998), as shown in Equation (3).

$$Unc = \begin{cases} \frac{5}{6} \times MDL; \; Conc. \leq MDL \\ \sqrt{(Error \; Fraction \times concentration)^2 + (0.5 \times MDL)^2}; \\ Conc. > MDL \end{cases} \tag{3}$$

where the *error fraction* is defined as 10% of the measured VOC concentrations (Hak et al., 2005; Yuan et al., 2012). The PMF analysis depends on the objective function (Q) to minimize the residual and uncertainty, as shown in Equation (4).
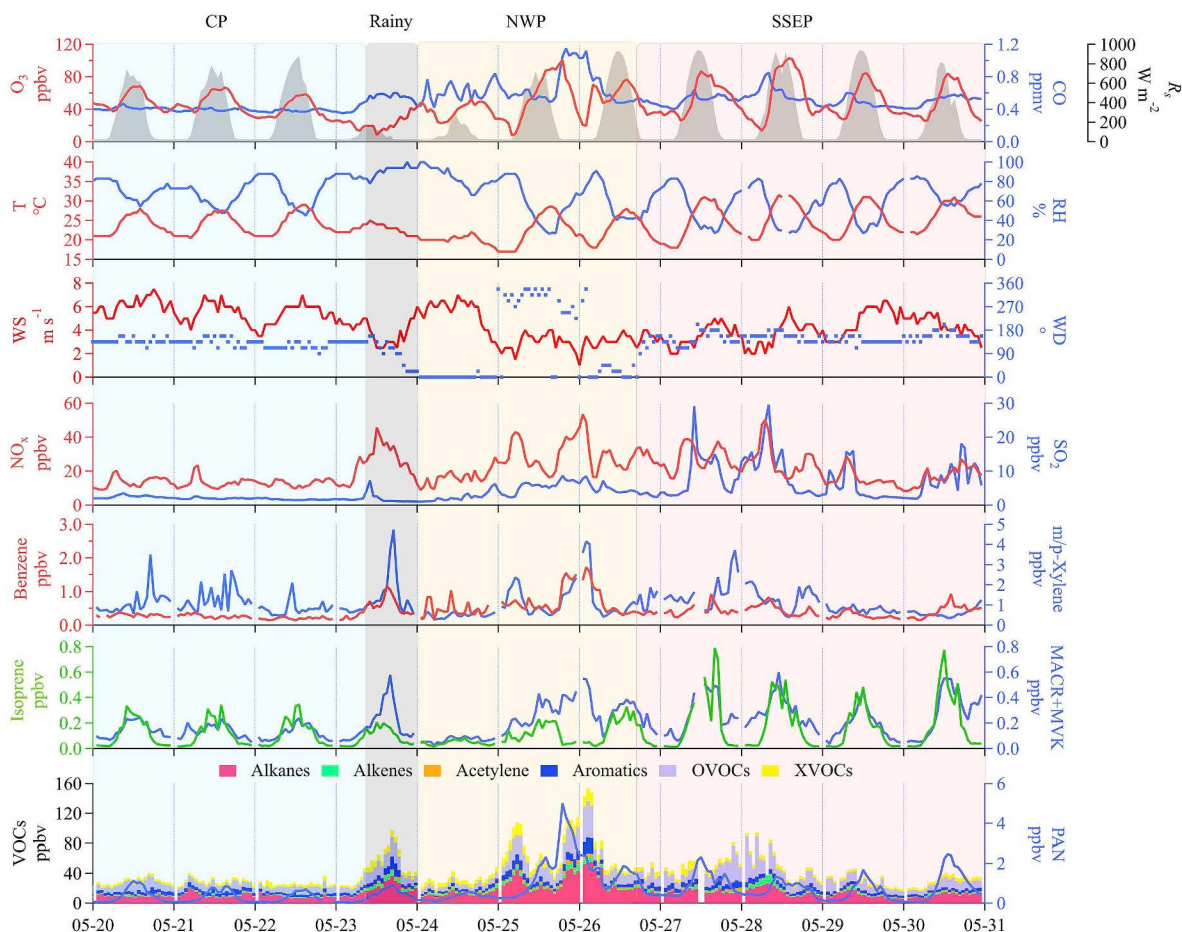

Fig. 1. Time series of meteorological parameters, trace gases and VOCs during the campaign. CP, NWP and SSEP represent clean period, northwest period and south-to-southeast period, respectively.

$$Q = \sum_{i=1}^{n} \sum_{j=1}^{m} \left[\frac{x_{ij} - \sum_{k=1}^{p} g_{ik} \times f_{kj}}{u_{ij}} \right]^2 \tag{4}$$

where n and m are the number of species and samples, respectively, and u_{ij} is the uncertainty of the jth species in the ith sample. Normally, monitoring the total Q is not meaningful because the expected value for a "good" solution ($Q_{\exp}$) depends on the size of the data matrix and on the number of chosen factors. The $Q/Q_{\exp}$ values can be used to choose the reasonableness of the model results (Song et al., 2019; Ulbrich et al., 2009). The calculation of $Q_{\exp}$ is shown in Equation (5).

$$Q_{\exp} = n \times m - p \times (n + m) \tag{5}$$

In this study, PMF factor numbers from 4 to 8 were explored for the best solution. We investigated a predefined F_{peak} range, i.e., from -5 to 5, and the results with nonzero F_{peak} values agree well with the zero F_{peak} values (Yuan et al., 2012). Quality indicators from the PMF application are summarized in Table S3. Fig. S4 shows the correlation between modeled VOC concentrations calculated using the contributions from all factors (vertical axis) with measured VOC concentrations (horizontal axis). A strong correlation ($r^2 = 0.98$) and the ratio of modeled vs. measured VOC (0.96) indicate that the PMF results can explain almost all the variance in measured VOC concentrations.

3. Results and discussion

3.1. Overview of the measurement results

Fig. 1 shows the time series of VOC species, trace gases (NO_x, CO, O_3 and PAN), and meteorological parameters (T, RH, WS, WD and R_s) in Shanghai from 20th to 30th of May 2017. During the campaign, the temperature ranged from 17.0 °C to 31.5 °C with an average of 23.7 ± 3.5 °C, RH varied from 27% to 100% (Table 1). The average wind speed was 4.4 ± 1.4 m s^{-1} with a maximum wind speed of 7.5 m s^{-1} during the day coming from the southeast on the 20th of May and the north on the 24th of May. The prevailing wind direction was coming from the southeast on most days but was interrupted by the invasion of a weak cold air system from the northwest of Shanghai between 23rd and 26th of May. During the invasion of the weak cold air system, Shanghai experienced an abrupt 5 °C decrease in T, rain from 11:00 on the 23rd of May to 24th of May and a significant increase in air pollutant concentrations from 18:00 on the 25th of May to 03:00 on the 26th of May. This increase in pollutant concentrations was most likely caused by the combined effects of regional transport and local accumulation under unfavorable meteorological conditions. As shown in

Fig. S5, the planetary boundary layer (PBL) height indicated by the vertical profile of aerosol extinction from a micro pulse LiDAR (MPL, Sigma Space Corporation) during the night of 25th to 26th was around 300 m, which also played important roles in the increase of air pollutant concentrations. After the passing of the cold air, the concentrations of most air pollutants sharply decreased when the WD changed back to the southeast, and the ambient T in Shanghai gradually rose from 26th to 30th of May. Although the winds were from the clean area over the East China Sea both before and after the invasion of the weak cold air system, the concentrations of most air pollutants were relatively higher during the later period. This difference could be explained by medium WSs and additional regional contributions from the south-to-southeast of Shanghai (where large petrochemical industries are located) (Fu et al., 2013; Huang et al., 2011) during the later period, as shown in Fig. 2.

During the campaign, the average concentration of VOCs in the atmosphere was 42.7 ± 23.0 ppbv in the order of alkanes (15.1 ± 9.0 ppbv) > OVOCs (13.5 ± 8.8 ppbv) > XVOCs (5.4 ± 3.0 ppbv) > aromatics (5.1 ± 2.9 ppbv) > alkenes (2.4 ± 1.9 ppbv) > acetylene (1.2 ± 0.9 ppbv). The top 10 species measured in this study including ethane, formaldehyde, propane, ethyl acetate, 1,4-dichlorobenzene, ethanol, n-butyl acetate, n-butane, dichloromethane and ethylene, which together comprised 52.5% of the total VOC concentration (Table S1).

Accordingly, the whole measurement period was divided into three periods, as shown in Fig. 1. During the first period (from 20th of May to 10:00 on the 23rd of May, areas shaded in light blue in Fig. 1), the prevailing wind in Shanghai was southeast wind from the relatively clean area of the East China Sea (Fig. 2a and b), and the average WS was 5.5 ± 0.9 m s^{-1}, which was higher than those during the other periods. Consequently, the concentrations of total VOCs (29.4 ± 6.2 ppbv), NO_x (13.9 ± 4.2 ppbv) and CO (0.40 ± 0.03 ppmv) were lower than those during other periods. The concentrations of photochemical products, i.e., O_3 and PAN, presented significant diurnal patterns with peaks at noon, and the peak values were lower during this period than on other days except 23rd of May and 24th of May, which featured rainy or cloudy conditions. We defined this period as a clean period (CP) characterized by low concentrations of air pollutants and influenced by clean air from the East China Sea and local emissions in Shanghai.

The second period was from 24th of May to 17:00 on the 26th of May (areas shaded in bright orange in Fig. 1), which corresponded to the invasion of the weak cold air system from the north-to-northwest of Shanghai, as mentioned above. This system resulted in rainy and cloudy
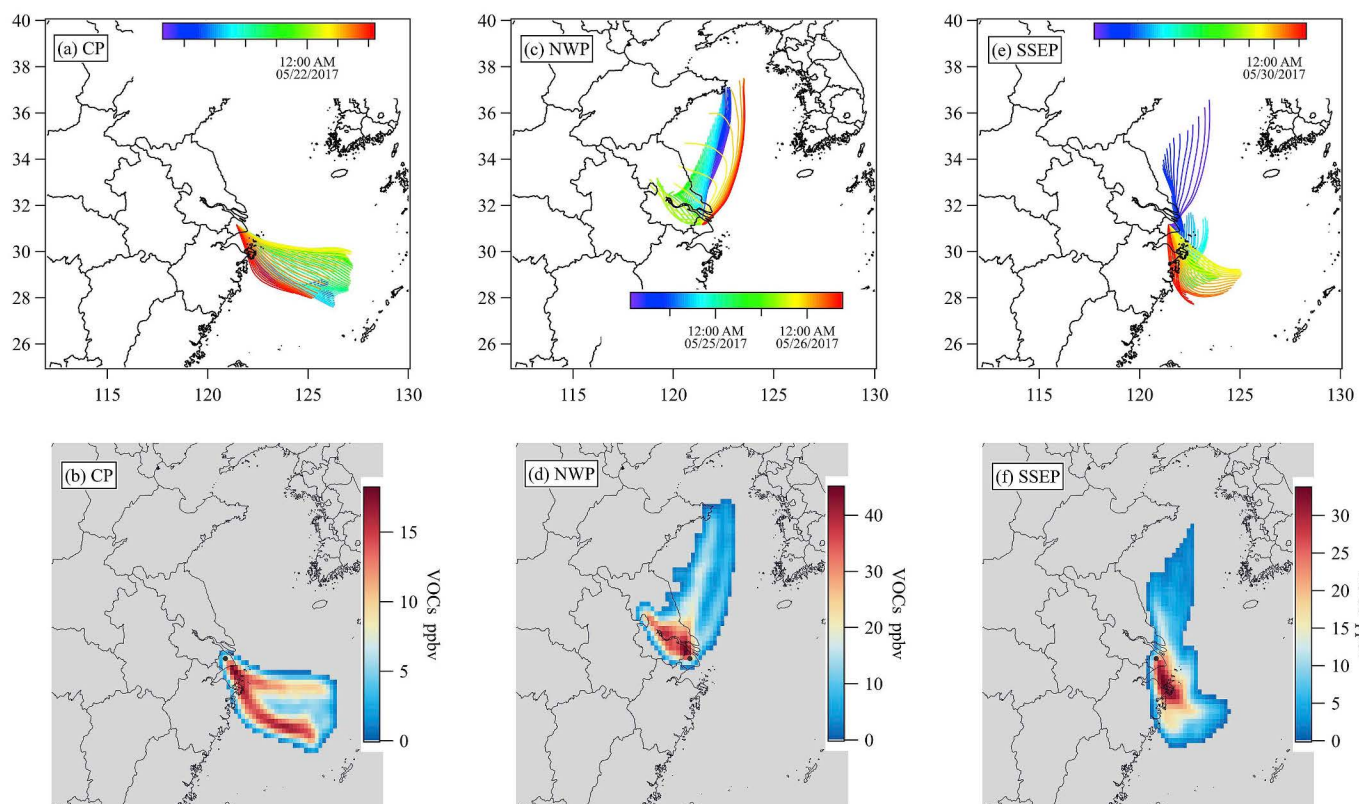
Table 1
Summary of meteorological parameters, trace gas and VOCs for different periods.

Species	CP[a]		NWP		SSEP	
	(5/20 - 5/23 10:00)		(5/24 - 5/26 17:00)		(5/26 18:00 - 5/30)	
	Range	Average ± SD	Range	Average ± SD	Range	Average ± SD
Meteorology data						
Temperature (°C)	20.5–29.0	23.9 ± 2.5	17.0–28.5	21.8 ± 3.4	18.0–31.5	25.1 ± 4.0
RH (%)	45–88	71.2 ± 12.7	27–100	68.3 ± 21.1	27–86	59.6 ± 18.5
WS (m s^{-1})	3.5–7.5	5.5 ± 0.9	1.0–7.0	3.9 ± 1.5	2.0–6.5	4.1 ± 1.1
Pollutants data (ppbv)						
O_3	13.4–68.6	42.7 ± 14.0	7.9–100.7	49.3 ± 21.5	13.6–102.9	50.9 ± 22.4
MDA8h O_3	–	52.3 ± 13.5	–	67.4 ± 16.7	–	79.3 ± 10.4
PAN	0.04–1.1	0.3 ± 0.3	0.07–5.0	1.2 ± 1.1	0.04–2.5	0.8 ± 0.6
NO_x	9.0–29.6	13.9 ± 4.2	9.0–53.4	24.8 ± 10.2	8.2–50.1	21.9 ± 8.6
NO_2	7.7–23.8	11.9 ± 3.4	7.4–50.7	21.8 ± 9.7	6.9–37.6	19.2 ± 7.3
NO	1.2–5.8	2.0 ± 1.0	1.3–10.0	2.9 ± 1.7	1.3–12.5	2.7 ± 2.2
SO_2	1.4–7.3	2.1 ± 0.7	1.1–8.6	4.2 ± 2.1	1.9–29.5	7.6 ± 5.9
CO (ppmv)	0.35–0.57	0.40 ± 0.03	0.42–1.15	0.65 ± 0.19	0.40–0.85	0.52 ± 0.08
VOCs	21.7–57.8	29.4 ± 6.2	20.1–153.6	57.5 ± 32.3	18.9–94.5	41.6 ± 16.6

[a] CP, NWP and SSEP represent clean period, northwest period and south-to-southeast period, respectively.

Fig. 2. (a, c, e) Clustered 24-h air mass backtrajectories starting at 100 m height for the NP, NWP and SSEP, respectively; (b, d, f) concentration weighted trajectory (CWT) maps for total VOCs for the NP, NWP and SSEP, respectively. The location of the sampling site is labeled by a black solid dot.

days during the early period with strong north wind and decreasing days-to-northwest WSs during the later period, as shown in Fig. 1. On the 23rd of May, both total VOC and NO$_x$ concentrations significantly increased due to the relatively stagnant air mass and in part to the presence of some pollution in the cold air front. The concentrations of air pollutants, except CO, were lower on the 24th of May than on the 23rd of May because of the strong north wind and then began to increase from the late 24th until the 26th of May with the decrease in WSs. In particular, the concentrations of most air pollutants reached their highest values around 02:00 on the 26th of May. The maximum VOC, NO$_x$ and CO hourly concentrations were as high as 153.6 ppbv, 53.4 ppbv and 1.15 ppmv, respectively. Regional transport from the north-northwest upwind of Shanghai, i.e., the Suzhou-Wuxi-Changzhou city cluster (Fig. 2c and d), as well as local accumulation due to relatively low WSs and low PBL heights, was probably the cause of the pollution discussed above, as indicated by the elevated PAN concentrations after sunset (Wang and Zhang, 2007). Thus, we defined the second period as the northwest period (NWP) because this pollution episode was influenced by regional transport from the northwest upwind of Shanghai and worsened by unfavorable dilution conditions meanwhile. Measurement data from 11:00 to 23:00 on the 23rd of May were excluded from analysis of the NWP in the discussion below due to rain.

The third period was from 18:00 on the 26th of May to 30th of May (areas shaded in light pink in Fig. 1), and after the cold air passed, Shanghai was under the influence of clean air from the sea again. However, the average concentrations of total VOCs, NO$_x$ and CO were higher than those during the CP, and in particular, the SO$_2$ concentrations reached the highest values among the three periods. This result was probably caused by medium WSs and the arrival of air masses from Ningbo-Zhoushan port (Fig. 2e and f), which features numerous petrochemical industrial parks and nonroad vehicle emissions located in the south-southeast upwind of Shanghai (Fan et al.,

2016; Liu et al., 2018a). The average concentrations of isoprene and its first-generation products, i.e., MACR and MVK, were also higher than those during the CP due to the higher Ts during the third period. Furthermore, all the diurnal peaks of R$_s$ were higher than those during the CP. As mentioned above, the meteorological conditions and higher concentrations of precursors promoted photochemical processes and led to additional O$_3$ and PAN formation. Accordingly, we defined the third period as the south-to-southeast period (SSEP) because this pollution episode was related to the combined results of local emissions and the upwind regional transport of pollutants from Ningbo-Zhoushan port, which is south to southeast of Shanghai.

3.2. VOC characteristics and potential source region

The VOC concentration, ozone formation potential (OFP) and their compositions during the three periods mentioned above are presented in Fig. 3. The values of OFP were calculated on the basis of the concentration of VOC species and multiplying its corresponding maximum incremental reactivity (MIR) updated in the Carter (2010) report. As shown in Fig. 3, the total VOC concentration was the highest during the NWP among the three periods and was 2.0 and 1.4 times higher than those during the CP and SSEP, respectively. In comparison, the total OFP during the NWP was 1.5 and 1.2 times higher than those during the CP and SSEP, respectively. Thus, the differences for OFP were less than those for the VOC concentrations. This result can be explained by the difference in composition among the three periods, suggesting that VOC species were more reactive to the formation of ozone during the CP than during the NWP and SSEP. As shown in Fig. 3, in all three periods, the most abundant species were alkanes, followed by OVOCs, XVOCs, aromatics, alkenes and acetylene, and their average concentration fractions were 35.1%, 32.0%, 12.7%, 11.9%, 5.6% and 2.8%, respectively. In comparison, for the OFP, the largest contribution species were aromatics, followed by OVOCs, alkanes, alkenes, XVOCs and acetylene,
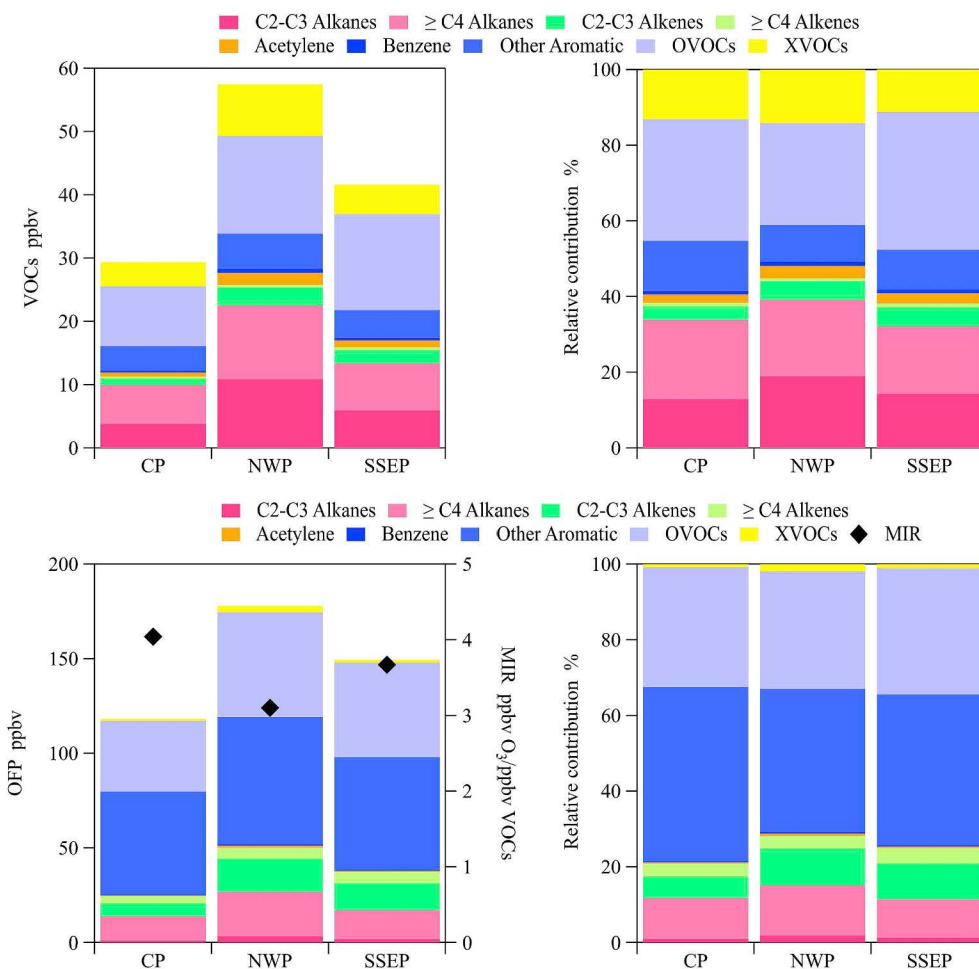
Fig. 3. The VOC concentrations, OFP and their compositions and average MIR during different periods.

and their average contribution fractions were 41.2%, 32.2%, 12.7%, 12.3%, 1.3% and 0.4%, respectively.

The VOC compositions presented some considerable differences among the three periods. First, the aromatic concentration fraction (14.2%) during the CP was the highest among all three periods and resulted in the highest ratio of total OFP to VOC concentration (the ratio can be estimated as the equivalent maximum incremental reactivity (MIR) of all VOC species) among the three periods (Fig. 4). As

shown in Fig. 2 and mentioned above, during the CP, Shanghai was mainly influenced by a clean air mass from sea, and thus, the measured VOCs were mainly from local emissions. Additionally, a high fraction of aromatics in the PAMS produced locally in Shanghai was reported in our previous study (Wang et al., 2013); this pattern is related to the abundant industrial solvent usage and chemical industry in Shanghai (Fu et al., 2013). The present results of the aromatic fraction in the PAMS are lower than the previous results in the study of Wang et al.
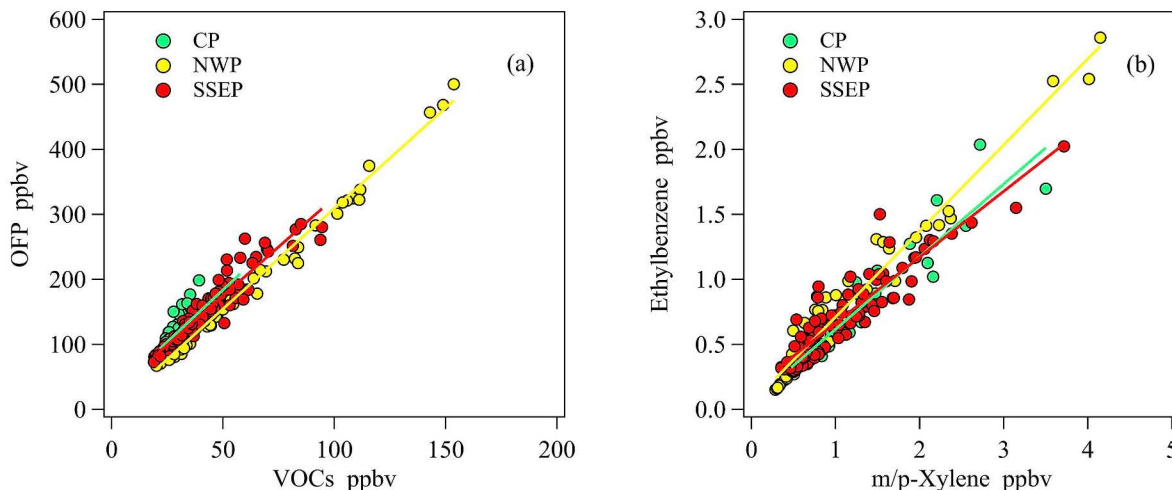

Fig. 4. Scatter plots of the VOC concentrations to OFP (a), and ethylbenzene to m/p-xylene (b) during different periods.

(2013), demonstrating the effectiveness of past multi-aromatic emission control measures in Shanghai. However, the aromatic fraction in the present study was still significantly higher than those in most cities in China (Huang et al., 2015; Hui et al., 2018; Li et al., 2015, 2017b, 2018, 2019a; Shao et al., 2016; Zou et al., 2015), as summarized in Table 2. This finding highlights the importance of controlling chemical and petrochemical industry emissions in Shanghai.

The second difference in VOC composition among the three periods was the higher fractions of alkanes and acetylene and lower fraction of OVOCs in the NWP than in the other two periods (Fig. 3). As shown in Fig. 2d, the VOCs in Shanghai during the NWP were mainly from local emissions and regional transport from the Suzhou-Wuxi-Changzhou city clusters, where abundant chemical industries are located and combustion processes occur (Zhao et al., 2017). The equivalent MIR was 3.10 ppbv O_3/ppbv VOCs during the NWP, as shown in Figs. 3 and 4a. These values during the NWP were lower than those during the other two periods. The ratio of ethylbenzene to m/p-xylene, which has been used to indicate the photochemical aging of an air mass (de Gouw, 2005), was 0.72 during the NWP, higher than those during the other two periods, as shown in Figs. 4b and 3. This finding suggests that regional transport brought relatively aged air masses and unreactive VOC species into Shanghai.

The top 10 highest contributors of OFP during the three periods are listed in Table 3. Generally, the species lists during different periods were similar, and the major contributors of OFP in Shanghai were aromatics with 7–9 carbons, carbonyls with 1–2 carbons, and alkenes with 2–3 carbons. Additionally, n-octane was also in the list of the top 10 contributors of OFP during the NWP, suggesting the importance of vehicle emissions (Kerschgens et al., 2016). As shown in Figs. 1 and 2, in the late period of the NWP, the WSs were relatively low, and these conditions were favorable to the accumulation of pollutants emitted near the ground. During the SSEP, acetates (i.e., n-butyl acetate and ethyl acetate) were also important contributors to the OFP and were probably from solvent use in the industrial parks located to the southeast of Shanghai and in Ningbo city (Fu et al., 2013; Li et al., 2014, 2017c). The species mentioned above together contributed approximately 60% of the OFP in Shanghai and were mainly from vehicle emissions and chemical and petrochemical industries (Ho et al., 2012; Legreid et al., 2007; Ma et al., 2016; Ou et al., 2015).

3.3. Source apportionment

3.3.1. Identification of PMF factors

Five sources, namely, solvent use, vehicle exhaust, biogenic, fuel evaporation, and aged air masses and secondary formation, were identified by the PMF model, and their source profiles and diurnal variation in source contributions are shown in Fig. 5 and Fig. 6, respectively.

Factor 1, shown in Fig. 5a, was rich in aromatic compounds, such as toluene (26.3% of the variation in this compound is explained by this factor; the percentages below have the same meaning), ethylbenzene (69.0%), m/p-xylene (74.6%), o-xylene (69.8%), and styrene (52.5%). The total contribution of these compounds is up to 72.3% to factor 1. The high abundances of these species (i.e., TEX) mainly originate from industrial processes and solvent use (Buzcu and Fraser, 2006; Ou et al., 2015; Yuan et al., 2010). In addition, this factor exhibited good covariation with n-butyl acetate and isopropyl alcohol (correlation coefficients $r = 0.64$ and 0.53, respectively; $p < 0.001$). These two compounds are most commonly used as solvents in industrial processes (Legreid et al., 2007; Zheng et al., 2013). It can also be noted that this factor shared little of its sources with combustion tracers, such as CO ($r = -0.05$), NO_x ($r = 0.18$) and acetylene ($r = 0.22$), suggesting that the contribution of combustion sources to this factor could be ignored. These support the assignment of this factor as the solvent use factor. The diurnal variation in solvent use exhibited higher concentrations during nighttime than during daytime (Fig. 6a), which could mainly be ascribed to strong photochemical consumption during the daytime. Meanwhile, the low PBL height during nighttime played important roles in high values at nighttime, and there might be some abnormal emissions at nighttime which were indicated by the higher standard deviations of values than those in daytime.

The source profile of factor 2, shown in Fig. 5b, was characterized by high proportions of alkenes, such as ethylene (72.8%), propylene (80.2%), 1-butene (75.3%), 1-pentene (38.2%), and acetylene (49.5%), which are important indicators of vehicle exhaust (Gentner et al., 2013; Harley and Kean, 2004; Löfgren and Petersson, 1992). Factor 2 was also characterized by relatively high proportions of C_2–C_6 alkanes (i.e., ethane, propane, iso/n-butanes and iso-pentane) and C_6–C_8 aromatics (i.e., benzene, toluene, m/p-xylene, o-xylene and styrene). These species are considered typical products of incomplete combustion processes (Baudic et al., 2016; Gaimoz et al., 2011; Liu et al., 2008a; Song et al., 2018). The diurnal emission profile of factor 2 was characterized by two peaks during traffic rush hours (Fig. 6b). Meanwhile, this factor had strong correlations with time series of NO_x and with CO ($r = 0.77$ and 0.78, respectively; $p < 0.001$), which are good tracers known to be highly related to vehicle exhaust (Baudic et al., 2016; Debevec et al., 2017; Huang et al., 2015). Therefore, factor 2 can be labeled vehicle exhaust. The average relative contribution of vehicle exhaust was 35.9%, which was the largest source of VOC emissions.

The source profile of factor 3, shown in Fig. 5c, was characterized by a particularly high proportion of isoprene (91.8%) but with a low abundance (7.1%). Isoprene is emitted from many plants (Monson

Table 2
Comparison of PAMS measured in Shanghai and other metropolitan areas in China.

Site	Type of site	Period	Interval	PAMS (ppbv)	Compositions of major groups (%)				Reference
					Alkanes	Alkenes	Acetylene	Aromatics	
Hongkong	urban	2011.05, 2011.08	24-hr	49.8	64.7	14.3	7.8	13.2	Huang et al. (2015)
Guangzhou	suburban	2012.05	1-hr	37.9	56.7	14.4	–	28.9	Zou et al. (2015)
Hangzhou	urban	2013.07.01–08.15	30 min	55.9	33.2	25.9	16.6	24.3	Li et al. (2017b)
Nanjing	suburban	2013.05.15–08.31	1-hr	34.4	43.5	21.4	8.8	26.3	Shao et al. (2016)
Chongqing	urban	2015.08.24–09.22	1-hr	41.2	59.1	15.9	9.4	15.5	Li et al. (2018)
Wuhan	urban	2017.06–08	1-hr	15.9	65	14.7	8.9	11.3	Hui et al. (2018)
Zhengzhou	urban	2017.05–09	7:00/14:00	29.2	56.7	14.1	12.9	16.2	Li et al. (2019a)
Beijing	urban	2014.05	1-hr	23.3	57.8	16.1	9.2	16.9	Li et al. (2015)
Shanghai	urban	2009.05, 2010.05	30 min	24.9	46.3	12.9	9.6	31.2	Wang et al. (2013)
Shanghai	urban	2017.05.20–05.30	1-hr	23.8	63.4	10.2	5.0	21.5	this study
				16.1	61.8	8.2	4.0	25.9	NP
				33.8	66.5	9.7	5.6	18.2	NWP
				21.8	61.4	11.6	5.0	22.0	SSEP

- Not detected or not listed.

Table 3
Top 10 highest contributors in OFP (ppbv) during different periods.

| CP		NWP		SSEP	
Species	Average ± SD	Species	Average ± SD	Species	Average ± SD
m/p-Xylene	19.4 ± 10.6	Formaldehyde	22.6 ± 12.3	m/p-Xylene	20.2 ± 12.1
Formaldehyde	13.9 ± 3.7	m/p-Xylene	18.3 ± 15.7	Formaldehyde	19.8 ± 9.1
Acetaldehyde	8.6 ± 5.1	Toluene	16.8 ± 14.8	Toluene	7.9 ± 5.3
o-Xylene	7.1 ± 3.8	Ethylene	12.2 ± 7.6	Ethylene	7.7 ± 6.0
Toluene	5.8 ± 2.7	Acetaldehyde	8.8 ± 4.2	o-Xylene	7.7 ± 4.2
Ethylbenzene	4.3 ± 2.3	o-Xylene	7.0 ± 5.5	Propylene	6.5 ± 9.2
Ethylene	4.1 ± 2.4	Propylene	5.3 ± 3.7	Acetaldehyde	6.0 ± 3.3
1,2,3-Trimethylbenzene	3.6 ± 0.9	Ethylbenzene	4.7 ± 3.8	Ethylbenzene	4.7 ± 2.5
1,2,4-Trimethylbenzene	3.0 ± 0.9	n-Octane	4.7 ± 4.1	n-Butyl acetate	4.5 ± 4.6
Propylene	2.6 ± 2.6	Ethanol	4.3 ± 3.0	Ethyl Acetate	4.5 ± 6.4
Σ Top 10	61.3%	Σ Top 10	58.1%	Σ Top 10	59.4%
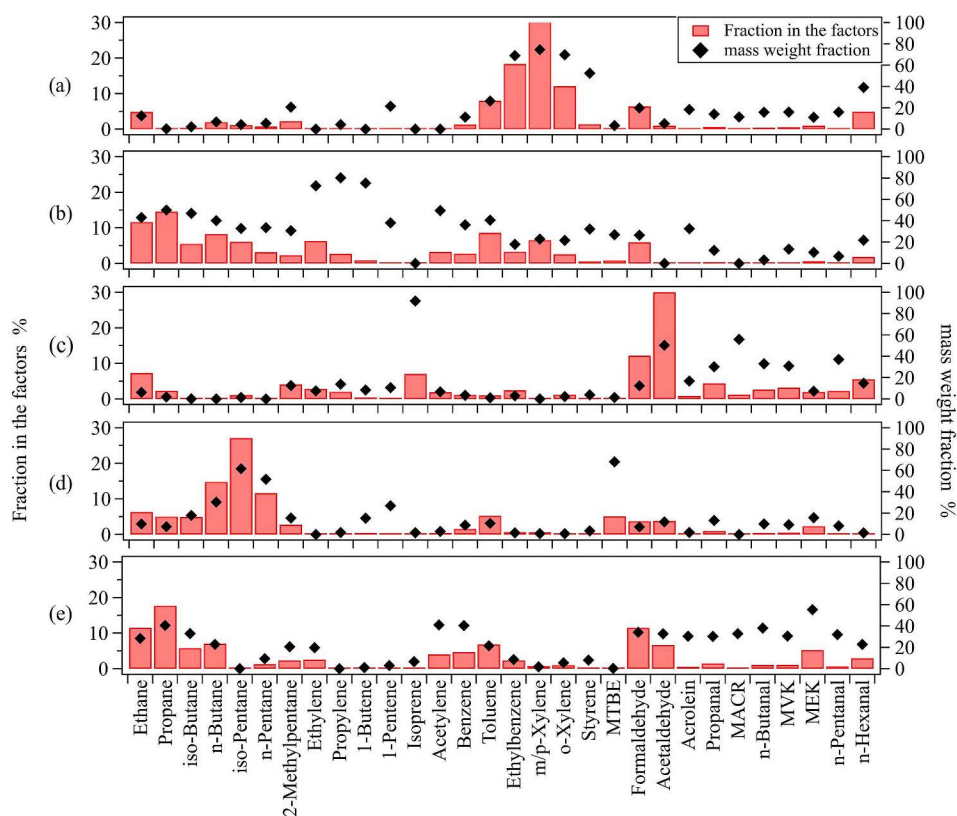
Fig. 5. Source profiles of the five-factor PMF solution, (a) factor 1 – solvent use, (b) factor 2 – vehicle exhaust, (c) factor 3 – biogenic, (d) factor 4 – fuel evaporation, (e) factor 5 – aged air masses and secondary formation. Red bar (left axis) indicate the mass fraction of individual species in each factor, and black square (right axis) show the mass weight fraction of each species apportioned to the factor. (For interpretation of the references to color in this figure legend, the reader is referred to the Web version of this article.)

et al., 2013) and is thought to be the most important biogenic hydrocarbon (Wennberg et al., 2018). Factor 3 also includes high proportions of intermediate products, such as acetaldehyde (Jardine et al., 2008; Winters et al., 2009), MACR and MVK. Thus, factor 3 was primarily attributed to biogenic emissions. The diurnal patterns of biogenic illustrated a clear T dependence (Fig. 6c), with high concentrations during daytime and low concentrations at night. The average relative contribution of this factor was 7.2%.

The source profile of factor 4, shown in Fig. 5d, was characterized by both high proportions and high abundances of n-butane and iso/n-pentanes, with more than 30% of their variabilities explained by this factor. These species have been identified (Gaimoz et al., 2011) and shown to be derived from gasoline components and evaporation sources (Lau et al., 2010; Salameh et al., 2014; Zhang et al., 2013), including storage, extraction, refueling losses, and distribution of gasoline (Debevec et al., 2017). The total contribution of these compounds to factor 4 was up to 58.7%. The contribution also included a considerable proportion of MTBE (68.1%), an exclusive tracer used as a fuel additive

in motor gasoline (Markus et al., 2010). Accordingly, we identified this factor as fuel evaporation. The independent traces used (i.e., NO_x and CO), appeared to exhibit poor correlations with the fuel evaporation factor ($r \leq 0.11$). The poor correlation between the fuel evaporation factor and the vehicle exhaust factor are also observed ($r = 0.12$, $p = 0.039$), indicating that these two factors did not share a common origin, e.g., road traffic as presented in the Baudic et al. (2016) study. Therefore, these compounds are expected to be derived from two mutually exclusive sources. The diurnal variation in fuel evaporation was characterized by an apparent increase in emissions from 03:00 to 06:00 and a much slower decrease in the evening between 20:00 and 21:00 (Fig. 6d). The average relative contribution of this factor was 13.4%.

The source profile of factor 5, as shown in Fig. 5e, was characterized by high proportions of relatively unreactive VOC species, such as ethane (28.5%), propane (40.5%), iso-butane (32.9%), n-butane (22.8%), acetylene (41.1%), benzene (40.5%) and MEK (55.4%), with their atmospheric lifetimes ranging from 5 to 47 days (Debevec et al., 2017). These species tend to accumulate in the urban atmosphere due
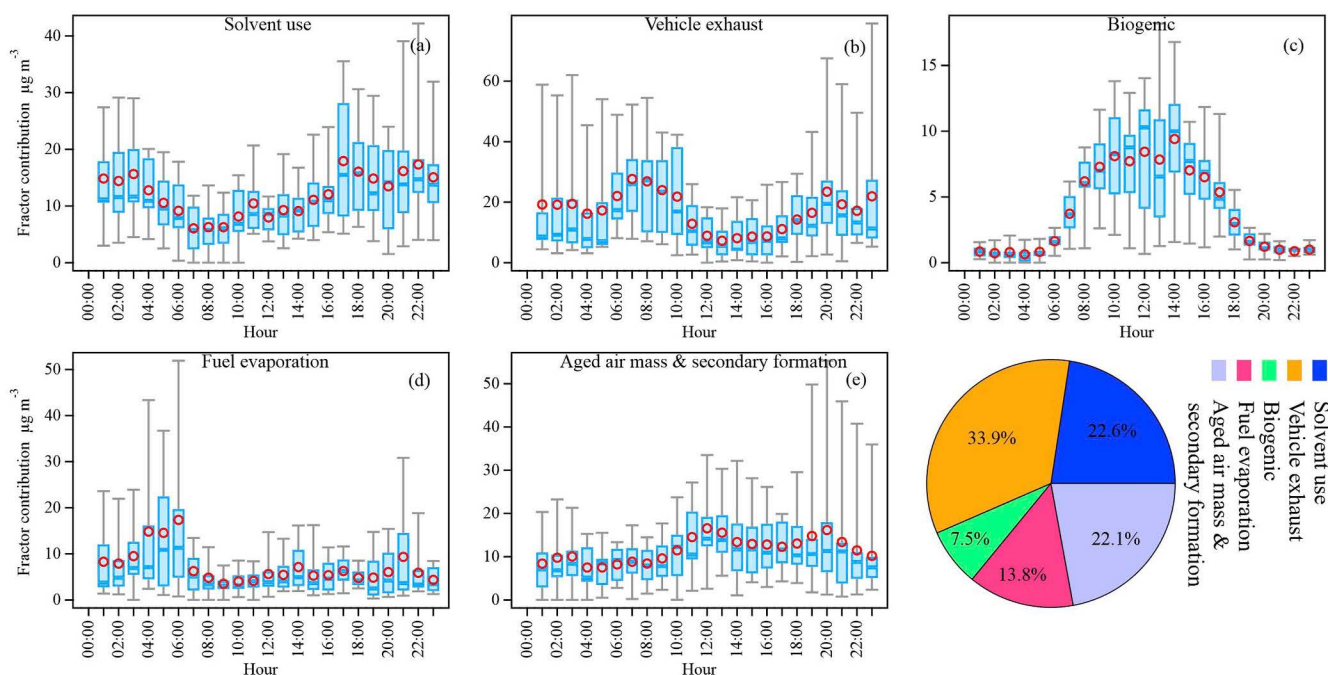
Fig. 6. Diurnal patterns of five factors from the PMF results, 25th and 75th percentile for deep sky-blue boxes, 5th and 95th percentile for whiskers, dashed lines for the median values, and solid red dots for the mean values. (For interpretation of the references to color in this figure legend, the reader is referred to the Web version of this article.)

to their low reactivities and have significant atmospheric background concentrations, especially in the Northern Hemisphere, and do not directly contribute to urban photochemical air pollution (Akimoto, 2016; Baudic et al., 2016). Factor 5 was well correlated with PAN ($r = 0.83$, $p < 0.01$), an important photochemical product (Lee et al., 2013; Nieboer and van Ham, 1976; Song et al., 2019). As shown in Fig. 5e, high abundances of formaldehyde and acetaldehyde in factor 5 could also be attributed to secondary formation (de Gouw, 2005). Thus, factor 5 was considered to be associated with aged air masses and secondary

formation. The diurnal variation in aged air masses and secondary formation was characterized by an increase in the concentrations at noon and the maintenance of relatively high concentrations until the evening. The diurnal profile of this factor (Fig. 6e) was relatively flat compared with the above four factors, and the slight increase during daytime was probably due to photochemical formation.

It should be noted that the blue line is drawn to solid circles in Fig. 8, which is the sigmoid fit line to the data points for non-methane hydrocarbon (NMHC) species. Yuan et al. (2012) proposed that if a
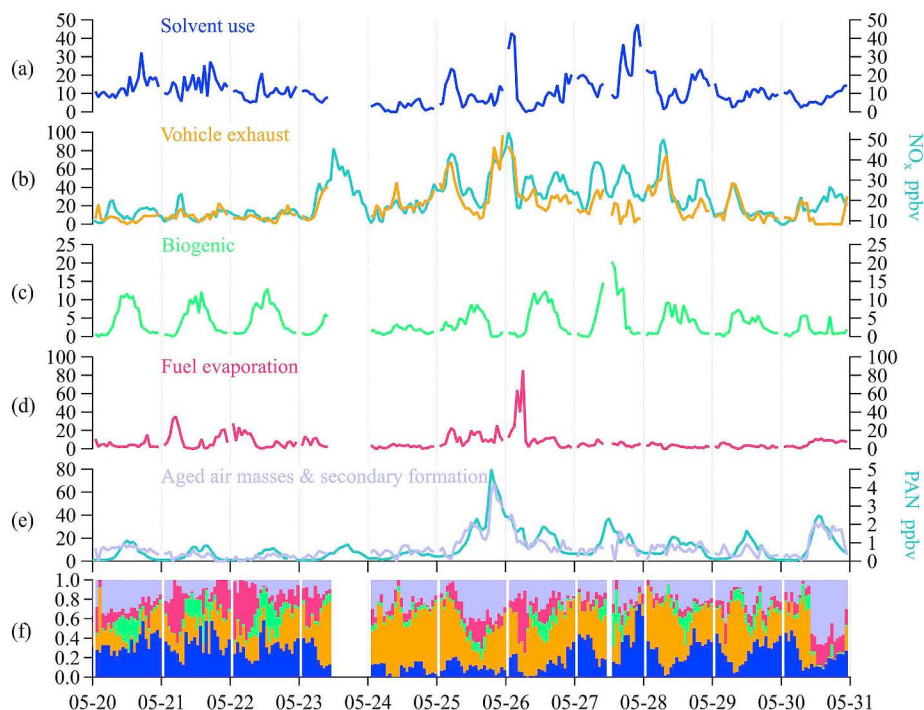

Fig. 7. Time series of the five factors mass contributions (a-e, $\mu g\ m^{-3}$) and accumulated relative VOC contributions (f).
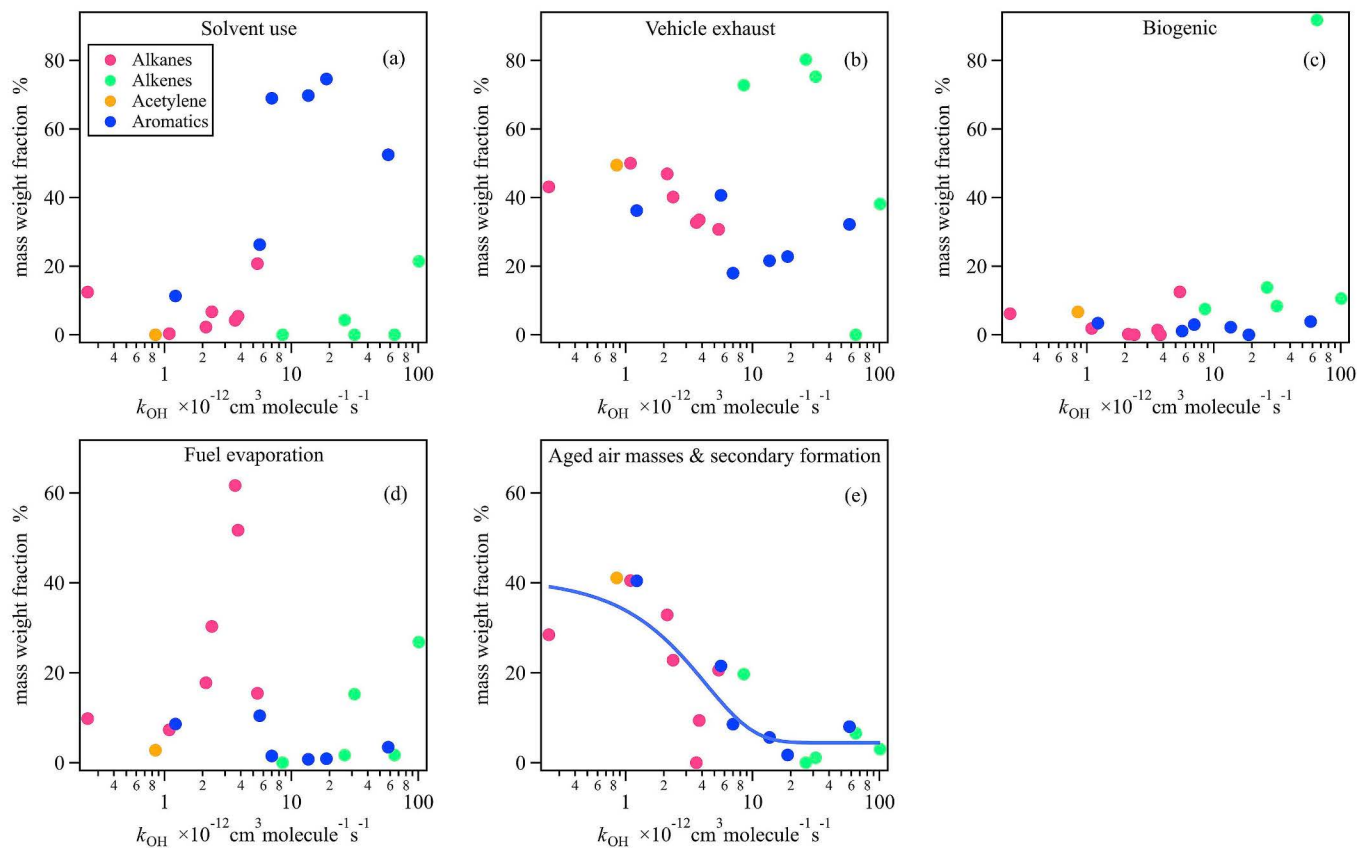
Fig. 8. Scattering points between factor fractions of NMHC species and their k_{OH} values. Each solid circle refers to one NMHC compound and is color-coded according to its chemical family (alkanes, alkenes, acetylene, aromatics). Blue line is the sigmoid fit line to the data points for NMHC species. (For interpretation of the references to color in this figure legend, the reader is referred to the Web version of this article.)
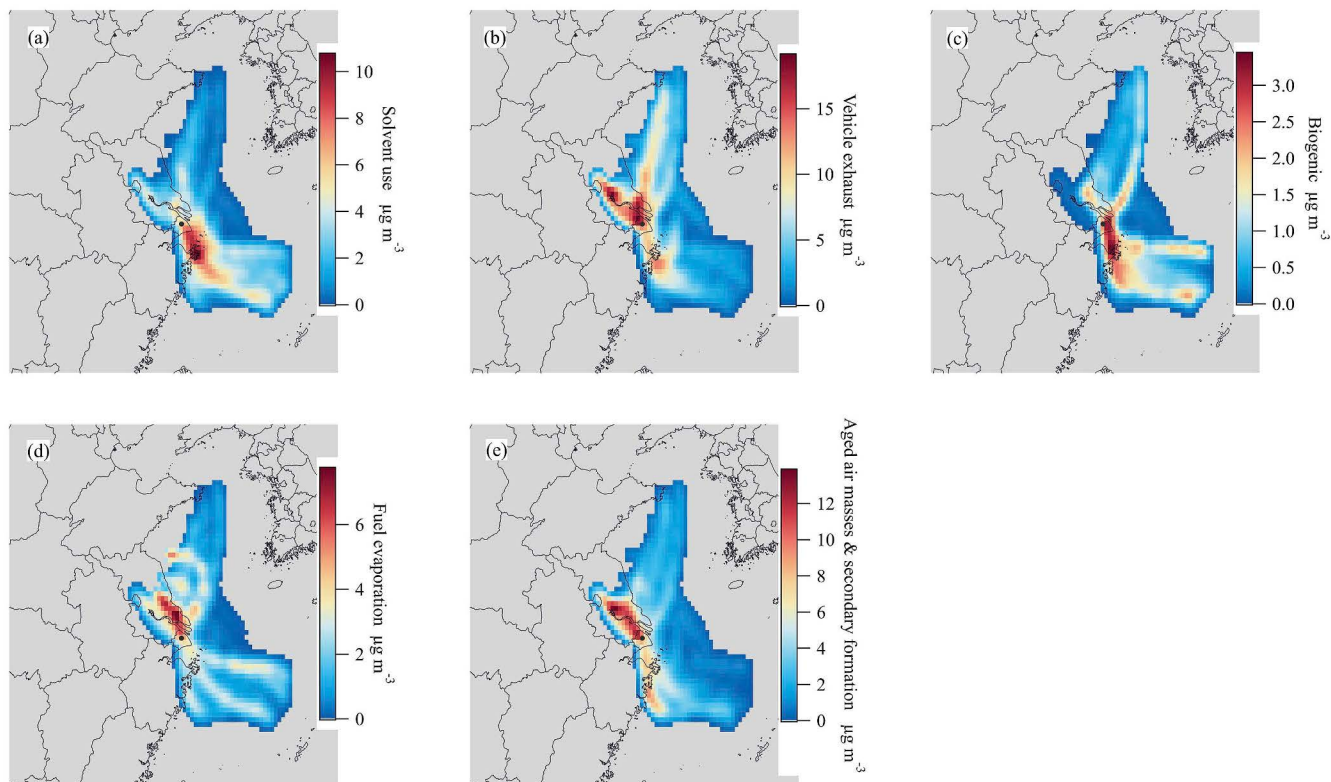

Fig. 9. CWT maps for sources of (a) solvent use, (b) vehicle exhaust, (c) biogenic, (d) fuel evaporation and (e) aged air masses and secondary formation.

factor extracted from the PMF model originates from a specific VOC source, then no dependence on photochemical processing is expected in Fig. 8. The PMF results for the VOC data set indicates that the aged air masses and secondary formation factor are a complex mix of VOC emission sources, which are strongly influenced by photochemistry as well as by the VOC sources; and the other four factors are not. As shown in Fig. 8e, the mass weight fractions of the aged air masses and secondary formation factor decreased as NMHCs became more reactive, and a good correlation between NMHC species and their k_{OH} values was excepted.

3.3.2. VOC source contributions

Time series of the VOC sources and their relative contributions to the VOC concentrations are presented in Fig. 7. As shown, peak values of solvent use appeared frequently during each period, and the highest concentration was observed at midnight on the 27th of May during the SSEP. This result suggested that solvent use VOCs were mainly from local emissions, as confirmed by the potential source region obtained by the CWT analysis and shown in Fig. 9a. On average, solvent use contributions ($\sim 12.5\,\mu g\,m^{-3}$) during the CP and SSEP were comparable and were significantly higher than those ($\sim 7.4\,\mu g\,m^{-3}$) during the NWP (Fig. 10). As a result, the relative contributions of solvent use were higher during the CP and SSEP at 31.4% and 25.6%, respectively, than during the NWP at 10.4% (Fig. 11). As expected, the time series of vehicle exhaust is similar to that of NO_x (Fig. 7b). Peak values were mainly observed during the late NWP and the early period of SSEP, during which the WSs were relatively low and not favorable to the diffusion of vehicle exhaust near the ground in urban areas. Consequently, the contribution of vehicle exhaust ($\sim 31.6\,\mu g\,m^{-3}$) during the NWP was much higher than that during the other two periods, accounting for 44.5% of VOCs during the NWP (Fig. 11). The CWT map also showed that vehicle exhaust was mainly from local emissions and the nearby areas to the north-to-northwest of Shanghai, specifically the Nantong and Suzhou-Wuxi-Changzhou city clusters. These areas together represent one of the most developed regions in China and contain numerous vehicles based on the data released by the Bureau of Statistics of Jiangsu Province (2018). Some sources of this factor were from the marine (Fig. 9b), which implied the contribution of ship emissions to VOCs in Shanghai under suitable meteorological conditions. On one hand, as reported, there were large amounts of VOC emissions from ships in the Shanghai and Ningbo-Zhoushan port and the East China Sea (Feng et al., 2019). On the other hand, there were some similarity of VOC species from on-road vehicle exhausts and ship emissions (Xiao et al., 2018), and it was not easy to separate them in source analysis.

Biogenic emissions present clear diurnal cycles with peaks around noon every day. On average, the concentrations ($\sim 3.8\,\mu g\,m^{-3}$) from biogenic emissions were comparable during the three periods (Fig. 10). The relative contributions to VOCs ranged from 5.0–10.7% (Fig. 11), being dependent on the variations in anthropogenic emissions. This result was comparable to that of a previous study in Shanghai (Wang et al., 2013). Some biogenic emissions were from the sea for biogenic emissions as shown in the CWT results (Fig. 9c), which was probably

due to the fact that marine organisms are mainly distributed in high marine eutrophic coastal areas and upwelling regions in the East China Sea, where more marine phytoplankton are produced in summer, thereby increasing isoprene emission (Li et al., 2017a).

Time series of fuel evaporation contributions exhibits several "spikes" during the CP and NWP (Fig. 7d), suggesting that there might be some leakage emissions of fuel storage in Shanghai and its surroundings in summer. On average, fuel evaporation contributed 19.0%, 15.0% and 8.2% of the VOCs during the CP, NWP and SSEP, respectively.

The temporal patterns of the contributions of the aged air masses and secondary formation are very similar to those of PAN, as shown in Fig. 7e. Generally, the contributions of the aged air masses and secondary formation were higher during the daytime than during the nighttime. The greatest contribution appeared at 19:00 on the 25th of May due to strong regional transport from the northwest of Shanghai (Fig. 9e). As a result, the relative contribution of the aged air masses and secondary formation was the highest during the NWP among the three periods, accounting for 25.1% of the VOCs (Fig. 11). The relative contribution of this source was also considerable during the SSEP due to strong photochemical processes, as mentioned in Section 3.1. Under the influence of the strong clean air mass from the East China Sea during the CP, the aged air masses and secondary formation contributed approximately 14.9% of the VOCs in Shanghai during the summer (Fig. 11).

In summary, vehicle emissions and chemical industries, especially industrial solvent usage, played the most important role in VOCs in urban Shanghai in summer, together accounting for more than 55% of VOCs. Regional transport and secondary formation were other important sources of VOCs, and their contribution ranged from $\sim 15\%$ to $\sim 25\%$ depending on the meteorological conditions, with an hourly maximum contribution as high as 67%. Fuel evaporation during storage should be considered, and leakage emissions might be an important source of fuel evaporation in Shanghai. Biogenic emissions were also considerable sources of VOCs in Shanghai during the summer.

3.4. Comparison with previous studies and emission inventories

As mentioned above, the VOC sources during the CP could be recognized as the local emissions, and the sources and their contributions were solvent use (31.4%), vehicle exhaust (24.0%), fuel evaporation (19.0%), biogenic emissions (10.7%), and aged air masses and secondary formation (14.9%). Compared to the previous results in the summer of 2009 and 2010 reported in Wang et al. (2013), the relative contribution of vehicle emissions decreased from 31.6% in summer of 2009 and 2010 to 24.0% in the summer of 2017, with a rapidly increasing trend of the average daily traffic volumes in urban Shanghai during these years (Data source: Shanghai Urban and Rural Construction and Transportation Development Research Institute), and the decrease in the relative contribution of vehicle emissions was mainly due to the out of use of the higher-emission vehicles in use and the more strict emissions standards of the new vehicles in Shanghai. The relative contribution of vehicles mentioned above was significantly higher than
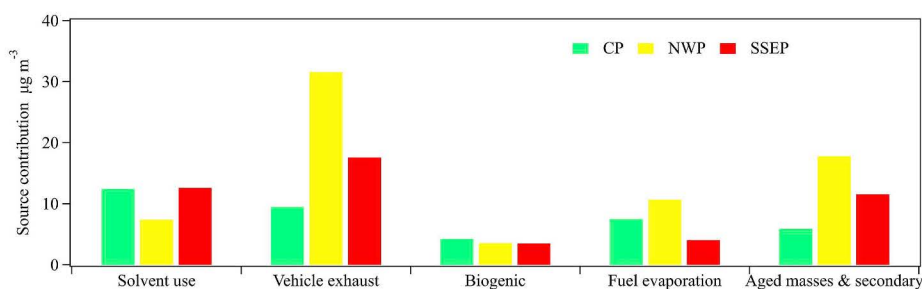

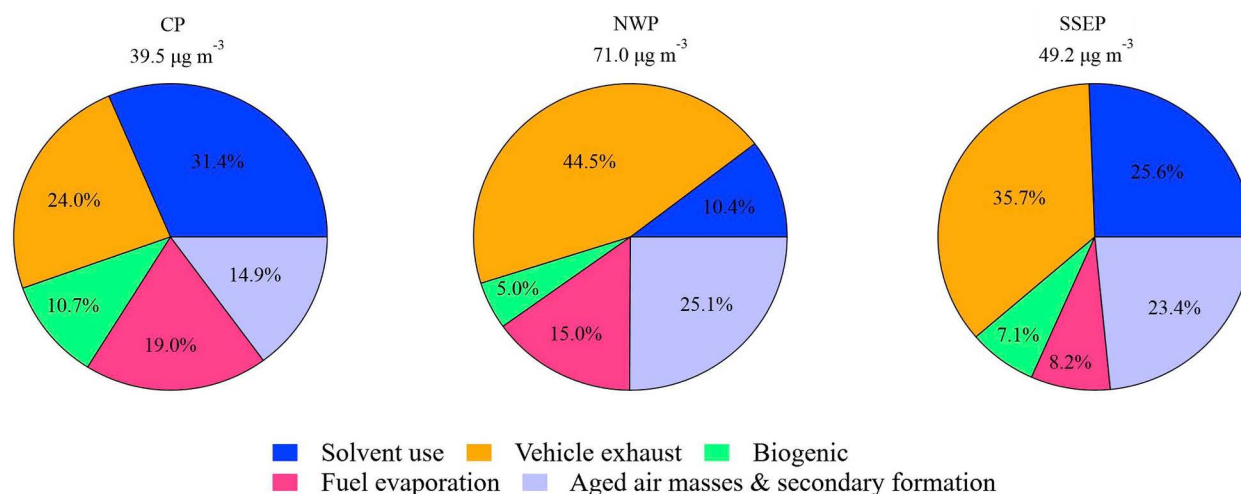**Fig. 10.** Comparison of source contributions to the VOCs during different periods.

Fig. 11. The relative contributions of the PMF-derived sources to the VOC mass loading during different periods.

that (13.5%) in the emission inventory (Wu and Xie, 2017), and one possible explanation was the present study carried out in the urban areas of Shanghai and the emission inventory covered the whole city.

Only two kinds of industrial sources were apportioned in this study, including solvent use (31.4%) and fuel evaporation (19.0%), which contributed 42.2% and 25.5%, respectively, to the primary sources obtained from the PMF results. Considering the poor correlation ($r = 0.11$, $p = 0.086$) between the fuel evaporation and NO_x, the fuel evaporation from the PMF results was mainly from the industries. The value of solvent use was similar to that (40.1%) in the emission inventory (Wu and Xie, 2017), and increased compared to the result of year 2009–2010 in Wang et al. (2013). While the relative contribution of fuel evaporation was much higher than that (4.3%) in the emission inventory (Wu and Xie, 2017), probably mixed by large emissions of chemical and petrochemical industries which were not identified in the PMF results. According to the emission inventory (Wu and Xie, 2017), the chemical and petrochemical industries as well as the industrial fuel evaporation took up 38% of the total emissions in Shanghai, which were much higher than that (25.5%) from the PMF results. Further studies such as the validation of VOC emission inventory were essential to get more insight into the chemical and petrochemical industrial emissions in Shanghai.

4. Conclusions

A field campaign was carried out from 20th to 30th of May 2017 in urban Shanghai, and three typical kinds of episodes were observed. Based on intensive measurements, including 108 VOC species, ozone and other trace gases, and meteorological parameters, VOC characteristics and sources were investigated with a focus on the relative contributions of local emissions and regional transport, as well as the potential source regions. The major conclusions were as follows.

Two kinds of episodes were observed during the present campaign when the prevailing wind was mainly from the East China Sea. In one kind of episode, Shanghai was mainly influenced by strong east-to-southeast winds from the clean sea area, which generally diluted the air pollution in Shanghai. During this episode, the VOCs were mainly from local emissions, and the concentrations were generally too low to induce ozone pollution. Specifically, solvent use and vehicle exhaust were the two largest sources of VOCs in Shanghai, with a combined contribution of 55.4%, followed by fuel evaporation mainly from fuel leakage (19.0%). Biogenic emissions were also considerable VOC sources, contributing approximately 10% of the VOCs. In the other kind of episode, the winds were mainly from the south-to-southeast direction and passed through the Ningbo-Zhoushan port area before arriving at

Shanghai, and the WSs of these winds were slightly lower than those from the east-to-southeast direction. During this episode, the VOCs observed in Shanghai were not only from local emissions, primarily chemical and petrochemical industrial emissions in southern Shanghai, but also from emissions from the Ningbo-Zhoushan port, which features numerous chemical and petrochemical industries and ship emissions. On average, regional transport contributed 23.4% of the VOCs during this kind of episode. The VOC concentrations were generally higher than those during periods dominated by the influence of east winds, which usually induced more ozone formation under unfavorable meteorological conditions.

In addition to the prevailing winds from the sea, northwest winds occurred frequently in Shanghai in early summer. The VOC emissions and their secondary products in areas upwind of Shanghai, specifically the Suzhou-Wuxi-Changzhou and Nantong city clusters, played an important role in the VOCs of Shanghai and easily resulted in a sharp increase in VOC concentrations. Meanwhile, the meteorological conditions in Shanghai became more stagnant in the late period, which were unfavorable to the dilution of local emissions. Thus, vehicle exhaust and regional aged air masses were the two most important sources of VOCs, together accounting for ~60%, while local industrial emissions mainly from the southern and eastern rural areas contributed relatively small amounts.

These results highlighted the importance of emission control of industrial solvent usage and vehicle exhaust, and fuel evaporation due to leakage should also be addressed in Shanghai. Furthermore, the regional transport of VOCs had a considerable contribution during the pollution episode, and joint control of VOCs with the surroundings, specifically the Suzhou-Wuxi-Changzhou and Nantong city clusters and Ningbo-Zhoushan port, is critical for Shanghai to improve its secondary air pollution.

Competing interests

The authors declare that they have no conflict of interest.

Acknowledgements

constructive comments, which have improved the paper.

Appendix A. Supplementary data

Supplementary data to this article can be found online at https://doi.org/10.1016/j.atmosenv.2019.116902.

References

Akimoto, H., 2016. Atmospheric Reaction Chemistry. Springer Atmospheric Sciences.

Atkinson, R., 2000. Atmospheric chemistry of VOCs and NO$_x$. Atmos. Environ. 34, 2063–2101.

Baudic, A., Gros, V., Sauvage, S., Locoge, N., Sanchez, O., Sarda-Estève, R., Kalogridis, C., Petit, J.-E., Bonnaire, N., Baisnée, D., Favez, O., Albinet, A., Sciare, J., Bonsang, B., 2016. Seasonal variability and source apportionment of volatile organic compounds (VOCs) in the Paris megacity (France). Atmos. Chem. Phys. 16, 11961–11989.

Bressi, M., Sciare, J., Ghersi, V., Mihalopoulos, N., Petit, J.E., Nicolas, J.B., Moukhtar, S., Rosso, A., Feron, A., Bonnaire, N., Poulakis, E., Theodosi, C., 2014. Sources and geographical origins of fine aerosols in Paris (France). Atmos. Chem. Phys. 14, 8813–8839.

Bureau of Statistics of Jiangsu Province, 2018. Jiangsu Statistical Yearbook 2018. China Statistics Press, Beijing.

Buzcu, B., Fraser, M.P., 2006. Source identification and apportionment of volatile organic compounds in Houston, TX. Atmos. Environ. 40, 2385–2400.

Carter, W., 2010. Updated Maximum Incremental Reactivity Scale and Hydrocarbon Bin Reactivities for Regulatory Applications. Prepared for California Air Resources Board Contract 07-339. College of Engineering Center for Environmental Research and Technology, University of California, Riverside, California.

Chan, K.L., Wang, S., Liu, C., Zhou, B., Wenig, M.O., Saiz-Lopez, A., 2017. On the summertime air quality and related photochemical processes in the megacity Shanghai, China. Sci. Total Environ. 580, 974–983.

Chan, L., Chu, K.W., Zou, S.C., Chan, C.Y., Wang, X.M., Barletta, B., Blake, D.R., Guo, H., Tsai, W.Y., 2006. Characteristics of nonmethane hydrocarbons (NMHCs) in industrial, industrial-urban, and industrial-suburban atmospheres of the Pearl River Delta (PRD) region of south China. J. Geophys. Res. Atmos. 111.

de Gouw, J.A., 2005. Budget of organic carbon in a polluted atmosphere: results from the new england air quality study in 2002. J. Geophys. Res. Atmos. 110 D16305.

Debevec, C., Sauvage, S., Gros, V., Sciare, J., Pikridas, M., Stavroulas, I., Salameh, T., Leonardis, T., Gaudion, V., Depelchin, L., Fronval, I., Sarda-Esteve, R., Baisnée, D., Bonsang, B., Savvides, C., Vrekoussis, M., Locoge, N., 2017. Origin and variability in volatile organic compounds observed at an Eastern Mediterranean background site (Cyprus). Atmos. Chem. Phys. 17, 11355–11388.

EPA, U.S., 1999. Determination of volatile organic compounds (VOCs). In: Air Collected in Specially-Prepared Canisters and Analyzed by Gas Chromatography-Ass Spectrometry (GCMS). U.S. Environmental Protection Agency, Washington, DC.

Fan, Q., Zhang, Y., Ma, W., Ma, H., Feng, J., Yu, Q., Yang, X., Ng, S.K.W., Fu, Q., Chen, L., 2016. Spatial and seasonal dynamics of ship emissions over the Yangtze River Delta and east China Sea and their potential environmental influence. Environ. Sci. Technol. 50, 1322–1329.

Feng, J., Zhang, Y., Li, S., Mao, J., Patton, A.P., Zhou, Y., Ma, W., Liu, C., Kan, H., Huang, C., An, J., Li, L., Shen, Y., Fu, Q., Wang, X., Liu, J., Wang, S., Ding, D., Cheng, J., Ge, W., Zhu, H., Walker, K., 2019. The influence of spatiality on shipping emissions, air quality and potential human exposure in the Yangtze River Delta/Shanghai, China. Atmos. Chem. Phys. 19, 6167–6183.

Fu, X., Wang, S., Zhao, B., Xing, J., Cheng, Z., Liu, H., Hao, J., 2013. Emission inventory of primary pollutants and chemical speciation in 2010 for the Yangtze River Delta region, China. Atmos. Environ. 70, 39–50.

Gaimoz, C., Sauvage, S., Gros, V., Herrmann, F., Williams, J., Locoge, N., Perrussel, O., Bonsang, B., d'Argouges, O., Sarda-Estève, R., Sciare, J., 2011. Volatile organic compounds sources in Paris in spring 2007. Part II: source apportionment using positive matrix factorisation. Environ. Chem. 8, 91–103.

Geng, F., Tie, X., Guenther, A., Li, G., Cao, J., Harley, P., 2011. Effect of isoprene emissions from major forests on ozone formation in the city of Shanghai, China. Atmos. Chem. Phys. 11, 10449–10459.

Gentner, D.R., Worton, D.R., Isaacman, G., Davis, L.C., Dallmann, T.R., Wood, E.C., Herndon, S.C., Goldstein, A.H., Harley, R.A., 2013. Chemical composition of gas-phase organic carbon emissions from motor vehicles and implications for ozone production. Environ. Sci. Technol. 47, 11837–11848.

Guo, H., Jiang, F., Cheng, H.R., Simpson, I.J., Wang, X.M., Ding, A.J., Wang, T.J., Saunders, S.M., Wang, T., Lam, S.H.M., Blake, D.R., Zhang, Y.L., Xie, M., 2009. Concurrent observations of air pollutants at two sites in the Pearl River Delta and the implication of regional transport. Atmos. Chem. Phys. 9, 7343–7360.

Guo, H., Wang, T., Blake, D.R., Simpson, I.J., Kwok, Y.H., Li, Y.S., 2006. Regional and local contributions to ambient non-methane volatile organic compounds at a polluted rural/coastal site in Pearl River Delta, China. Atmos. Environ. 40, 2345–2359.

Guo, P., Guo, K., Ren, Y., Shi, Y., Chang, J., Tani, A., Ge, Y., 2013. Biogenic volatile organic compound emissions in relation to plant carbon fixation in a subtropical urban–rural complex. Landsc. Urban Plan. 119, 74–84.

Hak, C., Pundt, I., Trick, S., Kern, C., Platt, U., Dommen, J., Ordóñez, C., Prévôt, A.S.H., Junkermann, W., Astorga-Lloréns, C., Larsen, B.R., Mellqvist, J., Strandberg, A., Yu, Y., Galle, B., Kleffmann, J., Lörzer, J.C., Braathen, G.O., Volkamer, R., 2005. Intercomparison of four different in-situ techniques for ambient formaldehyde measurements in urban air. Atmos. Chem. Phys. 5, 2881–2900.

Harley, R.A., Kean, A.J., 2004. Chemical Composition of Vehicle-Related Volatile Organic Compound Emission in Central Carlifonia (Draft Final Report). Prepared for: San Joaquin Valleywide Air Pollution Study Agency and California Air Resources Board. Department of Civil and Environmental Engineering, University of California, Berkeley, California.

Ho, S.S.H., Ho, K.F., Lee, S.C., Cheng, Y., Yu, J.Z., Lam, K.M., Feng, N.S.Y., Huang, Y., 2012. Carbonyl emissions from vehicular exhausts sources in Hong Kong. J. Air Waste Manag. Assoc. 62, 221–234.

Huang, C., Chen, C.H., Li, L., Cheng, Z., Wang, H.L., Huang, H.Y., Streets, D.G., Wang, Y.J., Zhang, G.F., Chen, Y.R., 2011. Emission inventory of anthropogenic air pollutants and VOC species in the Yangtze River Delta region, China. Atmos. Chem. Phys. 11, 4105–4120.

Huang, Y., Ling, Z.H., Lee, S.C., Ho, S.S.H., Cao, J.J., Blake, D.R., Cheng, Y., Lai, S.C., Ho, K.F., Gao, Y., Cui, L., Louie, P.K.K., 2015. Characterization of volatile organic compounds at a roadside environment in Hong Kong: an investigation of influences after air pollution control strategies. Atmos. Environ. 122, 809–818.

Hui, L., Liu, X., Tan, Q., Feng, M., An, J., Qu, Y., Zhang, Y., Jiang, M., 2018. Characteristics, source apportionment and contribution of VOCs to ozone formation in Wuhan, Central China. Atmos. Environ. 192, 55–71.

Jardine, K., Harley, P., Karl, T., Guenther, A., Lerdau, M., Mak, J.E., 2008. Plant physiological and environmental controls over the exchange of acetaldehyde between forest canopies and the atmosphere. Biogeosciences 5, 1559–1572.

Kerschgens, B., Cai, L., Pitsch, H., Heuser, B., Pischinger, S., 2016. Di-n-buthylether, n-octanol, and n-octane as fuel candidates for diesel engine combustion. Combust. Flame 163, 66–78.

Lau, A.K., Yuan, Z., Yu, J.Z., Louie, P.K., 2010. Source apportionment of ambient volatile organic compounds in Hong Kong. Sci. Total Environ. 408, 4138–4149.

Lee, J.B., Yoon, J.S., Jung, K., Eom, S.W., Chae, Y.Z., Cho, S.J., Kim, S.D., Sohn, J.R., Kim, K.H., 2013. Peroxyacetyl nitrate (PAN) in the urban atmosphere. Chemosphere 93, 1796–1803.

Legreid, G., Lööv, J.B., Staehelin, J., Hueglin, C., Hill, M., Buchmann, B., Prevot, A.S.H., Reimann, S., 2007. Oxygenated volatile organic compounds (OVOCs) at an urban background site in Zürich (Europe): seasonal variation and source allocation. Atmos. Environ. 41, 8409–8423.

Li, B., Ho, S.S.H., Gong, S., Ni, J., Li, H., Han, L., Yang, Y., Qi, Y., Zhao, D., 2019a. Characterization of VOCs and their related atmospheric processes in a central Chinese city during severe ozone pollution periods. Atmos. Chem. Phys. 19, 617–638.

Li, J., Zhai, C., Yu, J., Liu, R., Li, Y., Zeng, L., Xie, S., 2018. Spatiotemporal variations of ambient volatile organic compounds and their sources in Chongqing, a mountainous megacity in China. Sci. Total Environ. 627, 1442–1452.

Li, J.L., Zhang, H.H., Yang, G.P., 2017a. Distribution and sea-to-air flux of isoprene in the east China Sea and the south yellow Sea during summer. Chemosphere 178, 291–300.

Li, K., Chen, L., Ying, F., White, S.J., Jang, C., Wu, X., Gao, X., Hong, S., Shen, J., Azzi, M., Cen, K., 2017b. Meteorological and chemical impacts on ozone formation: a case study in Hangzhou, China. Atmos. Res. 196, 40–52.

Li, L., An, J., Huang, L., Yan, R., Huang, C., Yarwood, G., 2019b. Ozone source apportionment over the Yangtze River Delta region, China: investigation of regional transport, sectoral contributions and seasonal differences. Atmos. Environ. 202, 269–280.

Li, L., Xie, S., Zeng, L., Wu, R., Li, J., 2015. Characteristics of volatile organic compounds and their role in ground-level ozone formation in the Beijing-Tianjin-Hebei region, China. Atmos. Environ. 113, 247–254.

Li, M., Zhang, Q., Kurokawa, J., Woo, J.H., He, K.B., Lu, Z.F., Ohara, T., Song, Y., Streets, D.G., Carmichael, G.R., Cheng, Y.F., Hong, C.P., Huo, H., Jiang, X.J., Kang, S.C., Liu, F., Su, H., Zheng, B., 2017c. MIX: a mosaic Asian anthropogenic emission inventory under the international collaboration framework of the MICS-Asia and HTAP. Atmos. Chem. Phys. 17, 935–963.

Li, M., Zhang, Q., Streets, D.G., He, K.B., Cheng, Y.F., Emmons, L.K., Huo, H., Kang, S.C., Lu, Z., Shao, M., Su, H., Yu, X., Zhang, Y., 2014. Mapping Asian anthropogenic emissions of non-methane volatile organic compounds to multiple chemical mechanisms. Atmos. Chem. Phys. 14, 5617–5638.

Lindaas, J., Farmer, D.K., Pollack, I.B., Abeleira, A., Flocke, F., Roscioli, R., Herndon, S., Fischer, E.V., 2017. Changes in ozone and precursors during two aged wildfire smoke events in the Colorado Front Range in summer 2015. Atmos. Chem. Phys. 17, 10691–10707.

Liu, H., Meng, Z.H., Shang, Y., Lv, Z.F., Jin, X.X., Fu, M.L., He, K.B., 2018a. Shipping emission forecasts and cost-benefit analysis of China ports and key regions' control. Environ. Pollut. 236, 49–59.

Liu, Y., Li, L., An, J., Huang, L., Yan, R., Huang, C., Wang, H., Wang, Q., Wang, M., Zhang, W., 2018b. Estimation of biogenic VOC emissions and its impact on ozone formation over the Yangtze River Delta region, China. Atmos. Environ. 186, 113–128.

Liu, Y., Shao, M., Fu, L., Lu, S., Zeng, L., Tang, D., 2008a. Source profiles of volatile organic compounds (VOCs) measured in China: Part I. Atmos. Environ. 42, 6247–6260.

Liu, Y., Shao, M., Lu, S.H., Liao, C.C., Wang, J.L., Chen, G., 2008b. Volatile organic compound (VOC) measurements in the Pearl River Delta (PRD) region, China. Atmos. Chem. Phys. 8, 1531–1545.

Löfgren, L., Petersson, G., 1992. Butenes and butadiene in urban air. Sci. Total Environ. 116, 195–201.

Ma, Y., Diao, Y.W., Zhang, B.J., Wang, W.W., Ren, X.R., Yang, D.S., Wang, M., Shi, X.W., Zheng, J., 2016. Detection of formaldehyde emissions from an industrial zone in the Yangtze River Delta region of China using a proton transfer reaction ion-drift chemical ionization mass spectrometer. Atmos. Meas. Tech. 9, 6101–6116.

Markus, W., Ekkehard, S.K., Udo, P., Franz, N., 2010. Methyl Tert-Butyl Ether, Ullmann's Encyclopedia of Industrial Chemistry.

Monson, R.K., Jones, R.T., Rosenstiel, T.N., Schnitzler, J.P., 2013. Why only some plants

emit isoprene. Plant Cell Environ. 36, 503–516.

Nash, T., 1953. The colorimetric estimation of formaldehyde by means of the Hantzsch reaction. Biochem. J. 55, 416–421.

Nieboer, H., van Ham, J., 1976. Peroxyacetyl nitrate (PAN) in relation to ozone and some meteorological parameters at Delft in The Netherlands. Atmos. Environ. 10, 115–120 (1967).

Norris, G., Duvall, R., Brown, S., Bai, S., 2014. EPA Positive Matrix Factorization (PMF) 5.0 Fundamentals and User Guide Prepared for the. US Environmental Protection Agency Office of Research and Development, Washington, DC Inc., Petaluma).

Ou, J.M., Guo, H., Zheng, J.Y., Cheung, K., Louie, P.K.K., Ling, Z.H., Wang, D.W., 2015. Concentrations and sources of non-methane hydrocarbons (NMHCs) from 2005 to 2013 in Hong Kong: a multi-year real-time data analysis. Atmos. Environ. 103, 196–206.

Paatero, P., 1999. The multilinear engine—a table-driven, least squares Program for solving multilinear problems, including then-way parallel factor Analysis model. J. Comput. Graph. Stat. 8, 854–888.

Paatero, P., Tapper, U., 1994. Positive matrix factorization: a non-negative factor model with optimal utilization of error estimates of data values. Environmetrics 5, 111–126.

Petit, J.E., Favez, O., Albinet, A., Canonaco, F., 2017. A user-friendly tool for comprehensive evaluation of the geographical origins of atmospheric pollution: wind and trajectory analyses. Environ. Model. Softw 88, 183–187.

Polissar, A.V., Hopke, P.K., Paatero, P., Malm, W.C., Sisler, J.F., 1998. Atmospheric aerosol over Alaska: 2. Elemental composition and sources. J. Geophys. Res. Atmos. 103, 19045–19057.

Preunkert, S., Legrand, M., Pépy, G., Gallée, H., Jones, A., Jourdain, B., 2013. The atmospheric HCHO budget at Dumont d'Urville (East Antarctica): contribution of photochemical gas-phase production versus snow emissions. J. Geophys. Res. Atmos. 118, 13319–13337.

Ran, L., Zhao, C., Geng, F., Tie, X., Tang, X., Peng, L., Zhou, G., Yu, Q., Xu, J., Guenther, A., 2009. Ozone photochemical production in urban Shanghai, China: analysis based on ground level observations. J. Geophys. Res. Atmos. 114.

Salameh, T., Afif, C., Sauvage, S., Borbon, A., Locoge, N., 2014. Speciation of non-methane hydrocarbons (NMHCs) from anthropogenic sources in Beirut, Lebanon. Environ. Sci. Pollut. Res. 21, 10867–10877.

Seinfeld, J.H., Pandis, S.N., 2016. Atmospheric Chemistry and Physics: from Air Pollution to Climate Change, third ed. John Wiley & Sons.

Shanghai Municipal Statistics Bureau, 2018. Shanghai Statistical Yearbook 2018. Shanghai Municipal Statistics Bureau, China Statistics Press, Beijing.

Shao, P., An, J., Xin, J., Wu, F., Wang, J., Ji, D., Wang, Y., 2016. Source apportionment of VOCs and the contribution to photochemical ozone formation during summer in the typical industrial area in the Yangtze River Delta, China. Atmos. Res. 176–177, 64–74.

Song, M., Liu, X., Zhang, Y., Shao, M., Lu, K., Tan, Q., Feng, M., Qu, Y., 2019. Sources and abatement mechanisms of VOCs in southern China. Atmos. Environ. 201, 28–40.

Song, M., Tan, Q., Feng, M., Qu, Y., Liu, X., An, J., Zhang, Y., 2018. Source apportionment and secondary transformation of atmospheric non-methane hydrocarbons in Chengdu, southwest China. J. Geophys. Res. Atmos. 123, 9741–9763.

Spaulding, R.S., Schade, G.W., Goldstein, A.H., Charles, M.J., 2003. Characterization of secondary atmospheric photooxidation products: evidence for biogenic and anthropogenic sources. J. Geophys. Res. Atmos. 108.

Tie, X., Geng, F., Guenther, A., Cao, J., Greenberg, J., Zhang, R., Apel, E., Li, G., Weinheimer, A., Chen, J., Cai, C., 2013. Megacity impacts on regional ozone formation: observations and WRF-Chem modeling for the MIRAGE-Shanghai field campaign. Atmos. Chem. Phys. 13, 5655–5669.

Ulbrich, I.M., Canagaratna, M.R., Zhang, Q., Worsnop, D.R., Jimenez, J.L., 2009. Interpretation of organic components from Positive Matrix Factorization of aerosol mass spectrometric data. Atmos. Chem. Phys. 9, 2891–2918.

Wagner, P., Kuttler, W., 2014. Biogenic and anthropogenic isoprene in the near-surface urban atmosphere — a case study in Essen, Germany. Sci. Total Environ. 475, 104–115.

Waked, A., Favez, O., Alleman, L.Y., Piot, C., Petit, J.E., Delaunay, T., Verlinden, E., Golly, B., Besombes, J.L., Jaffrezo, J.L., Leoz-Garziandia, E., 2014. Source apportionment of PM$_{10}$ in a north-western Europe regional urban background site (Lens, France) using positive matrix factorization and including primary biogenic emissions. Atmos. Chem. Phys. 14, 3325–3346.

Wang, B., Zhang, J.B., 2007. Monitoring and analysis of PAN and PPN in the air of Beijing

during the summer of 2005. Environ. Sci. 28, 1621–1626.

Wang, H.L., Chen, C.H., Wang, Q., Huang, C., Su, L.Y., Huang, H.Y., Lou, S.R., Zhou, M., Li, L., Qiao, L.P., Wang, Y.H., 2013. Chemical loss of volatile organic compounds and its impact on the source analysis through a two-year continuous measurement. Atmos. Environ. 80, 488–498.

Wang, M., Zeng, L., Lu, S., Shao, M., Liu, X., Yu, X., Chen, W., Yuan, B., Zhang, Q., Hu, M., Zhang, Z., 2014. Development and validation of a cryogen-free automatic gas chromatograph system (GC-MS/FID) for online measurements of volatile organic compounds. Anal. Methods 6, 9424–9434.

Wei, W., Li, Y., Wang, Y., Cheng, S., Wang, L., 2018. Characteristics of VOCs during haze and non-haze days in Beijing, China: concentration, chemical degradation and regional transport impact. Atmos. Environ. 194, 134–145.

Wennberg, P.O., Bates, K.H., Crounse, J.D., Dodson, L.G., McVay, R.C., Mertens, L.A., Nguyen, T.B., Praske, E., Schwantes, R.H., Smarte, M.D., St Clair, J.M., Teng, A.P., Zhang, X., Seinfeld, J.H., 2018. Gas-Phase reactions of isoprene and its major oxidation products. Chem. Rev. 118, 3337–3390.

Winters, A.J., Adams, M.A., Bleby, T.M., Rennenberg, H., Steigner, D., Steinbrecher, R., Kreuzwieser, J., 2009. Emissions of isoprene, monoterpene and short-chained carbonyl compounds from Eucalyptus spp. in southern Australia. Atmos. Environ. 43, 3035–3043.

Wu, R., Xie, S., 2017. Spatial distribution of ozone formation in China derived from emissions of speciated volatile organic compounds. Environ. Sci. Technol. 51, 2574–2583.

Xiao, Q., Li, M., Liu, H., Fu, M., Deng, F., Lv, Z., Man, H., Jin, X., Liu, S., He, K., 2018. Characteristics of marine shipping emissions at berth: profiles for particulate matter and volatile organic compounds. Atmos. Chem. Phys. 18, 9527–9545.

Xue, L.K., Wang, T., Gao, J., Ding, A.J., Zhou, X.H., Blake, D.R., Wang, X.F., Saunders, S.M., Fan, S.J., Zuo, H.C., Zhang, Q.Z., Wang, W.X., 2014. Ground-level ozone in four Chinese cities: precursors, regional transport and heterogeneous processes. Atmos. Chem. Phys. 14, 13175–13188.

Yang, X., Xue, L., Wang, T., Wang, X., Gao, J., Lee, S., Blake, D.R., Chai, F., Wang, W., 2018. Observations and explicit modeling of summertime carbonyl formation in beijing: identification of key precursor species and their impact on atmospheric oxidation chemistry. J. Geophys. Res. Atmos. 123, 1426–1440.

Yuan, B., Shao, M., de Gouw, J., Parrish, D.D., Lu, S., Wang, M., Zeng, L., Zhang, Q., Song, Y., Zhang, J., Hu, M., 2012. Volatile organic compounds (VOCs) in urban air: how chemistry affects the interpretation of positive matrix factorization (PMF) analysis. J. Geophys. Res. Atmos. 117.

Yuan, B., Shao, M., Lu, S., Wang, B., 2010. Source profiles of volatile organic compounds associated with solvent use in Beijing, China. Atmos. Environ. 44, 1919–1926.

Zhang, J., Wang, T., Chameides, W.L., Cardelino, C., Blake, D.R., Streets, D., 2008. Source characteristics of volatile organic compounds during high ozone episodes in Hong Kong, Southern China. Atmos. Chem. Phys. 8, 4983–4996.

Zhang, Y., Wang, X., Zhang, Z., Lü, S., Shao, M., Lee, F.S.C., Yu, J., 2013. Species profiles and normalized reactivity of volatile organic compounds from gasoline evaporation in China. Atmos. Environ. 79, 110–118.

Zhao, Y., Mao, P., Zhou, Y., Yang, Y., Zhang, J., Wang, S., Dong, Y., Xie, F., Yu, Y., Li, W., 2017. Improved provincial emission inventory and speciation profiles of anthropogenic non-methane volatile organic compounds: a case study for Jiangsu, China. Atmos. Chem. Phys. 17, 7733–7756.

Zheng, C., Shen, J., Zhang, Y., Huang, W., Zhu, X., Wu, X., Chen, L., Gao, X., Cen, K., 2017a. Quantitative assessment of industrial VOC emissions in China: historical trend, spatial distribution, uncertainties, and projection. Atmos. Environ. 150, 116–125.

Zheng, J., Garzón, J.P., Huertas, M.E., Zhang, R., Levy, M., Ma, Y., Huertas, J.I., Jardón, R.T., Ruíz, L.G., Tan, H., Molina, L.T., 2013. Volatile organic compounds in Tijuana during the Cal-Mex 2010 campaign: measurements and source apportionment. Atmos. Environ. 70, 521–531.

Zheng, J., Hu, M., Du, Z., Shang, D., Gong, Z., Qin, Y., Fang, J., Gu, F., Li, M., Peng, J., Li, J., Zhang, Y., Huang, X., He, L., Wu, Y., Guo, S., 2017b. Influence of biomass burning from South Asia at a high-altitude mountain receptor site in China. Atmos. Chem. Phys. 17, 6853–6864.

Zou, Y., Deng, X.J., Zhu, D., Gong, D.C., Wang, H., Li, F., Tan, H.B., Deng, T., Mai, B.R., Liu, X.T., Wang, B.G., 2015. Characteristics of 1 year of observational data of VOCs, NO$_x$ and O$_3$ at a suburban site in Guangzhou, China. Atmos. Chem. Phys. 15, 6625–6636.